6MW, 10kV HIGH SPEED PMSM DIGITAL DRIVE SYSTEM FOR HIGHLY EFFICIENT COMPRESSORS

Paper No. PCIC energy EUR24_10

Jörg Janning
Wolong GRC
Schwalmstr. 289
41238 Mönchengladbach
Germany

Pengcheng Zhu
Wolong GRC
No1801 West Renmin Rd.
312300 Shaoxing
Zhejiang, China

Chunzhi Deng
Wolong GRC
No1801 West Renmin Rd.
312300 Shaoxing
Zhejiang, China

Abstract – Modern gas compressor systems in the megawatt range strive for high reliability and efficiency. High speed motors with active magnetic bearings (AMB) can be directly coupled to the compressor without need of a gearbox. This technology has already been applied utilizing high speed induction motors.
The paper outlines a new digital drive solution utilizing a permanent magnet synchronous motor (PMSM) with a power of 6MW fed by a 10kV multilevel medium voltage inverter. Measurement and simulation results show a significant efficiency improvement. The inverter is designed for high reliability with built-in redundancy reaching MTBF values of more than 14 years. The inverter topology is compared with known solutions and the specific requirements of the PMSM motor are explained.
Digital drive train functionalities such as predictive maintenance and virtual commissioning are evaluated. Utilizing digital twins, the drive system can proactively anticipate anomalies and generate alerts.
The paper concludes with the feasible power range of this drive solution for compressor applications, indicating the potential energy savings and CO2 reduction.

Index Terms — High speed drives, Compressors, Multilevel, Digital drive.

I. INTRODUCTION

High speed drives are gaining more and more importance as they allow to dispense gearboxes improving the overall efficiency and reliability of the application. Typical applications are in electric vehicles, HVAC and compressors. Gas compressor applications for pipelines and storage have higher power demand. The majority of compressor lines are still driven with geared solutions or even with gas motors. High power and high-speed compressor lines with induction motors meanwhile have a long track record. The induction motor and gas compressor can be realized in two separate and coupled units or integrated in one housing and cooled with process gas. These integrated compressor lines (ICL) are the most advanced solution. The overall compactness of an ICL compressor system is improved by 50%.

This paper describes a high-speed drive system using a permanent magnet synchronous motor (PMSM) fed by a multilevel inverter. Compared to the induction motor the PMSM has the advantage of not needing to excite the rotor via the stator which results in a higher efficiency. Typically, PMSM motors are known from applications with lower power like EV drives and are not built in the high-power range of 6MW and more as presented here. The PMSM rotor has surface mounted permanent magnets and no built-in damper cage. With this the rotor has very low losses. However, the PMSM requires very low current harmonics as these harmonics would otherwise heat up the rotor. The presented 6MW drive system is utilizing a 10kV multilevel inverter feeding the PMSM motor with a frequency of 333Hz at 10000rpm. With this it is one of the largest high—speed PMSM drives in the world.

The paper describes the motor design and the inverter feeding the motor. It further discusses why the selected inverter is well fitting to this application and compares the overall efficiency of the drive system with a comparable solution with high-speed induction motors.

The typical application of this drive system requires a high reliability. Therefore, the paper outlines how the reliability of the inverter can be increased by utilizing redundancy and how this is supported by the control. Further, the behavior at grid faults is outlined.

Reliability strongly depends on early detection of faults and predictive maintenance. It is explained how the drive system is prepared for these digital features. This includes precise simulation models for system engineering, monitoring, and fault diagnosis.

II. INVERTER AND MOTOR DESIGN

The high speed PMSM motor with 4 poles is running at a very high output frequency of 333.4Hz (see table 1). Each quarter section holds one surface mounted pole (figure 1).

Rated power	6	MW
Rated stator voltage	10	kV
Rated stator current	350	A
Power factor	1	
Rated stator frequency	333.4	Hz
Number of poles	4	
Insulation class	H	
Frame size	450	Mm

Table 1 Efficiency comparison of PMSM and CHB inverter with conventional induction motor drives

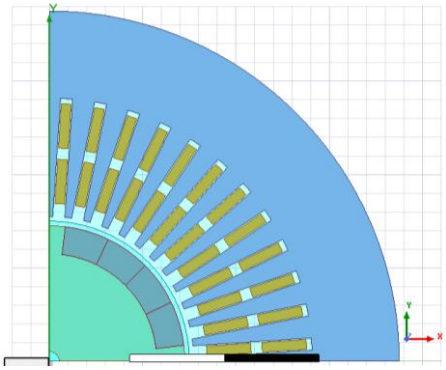

Fig. 1 2D cut through the PMSM motor (quarter section)

Fig. 2 Cascaded H-bridge inverter topology

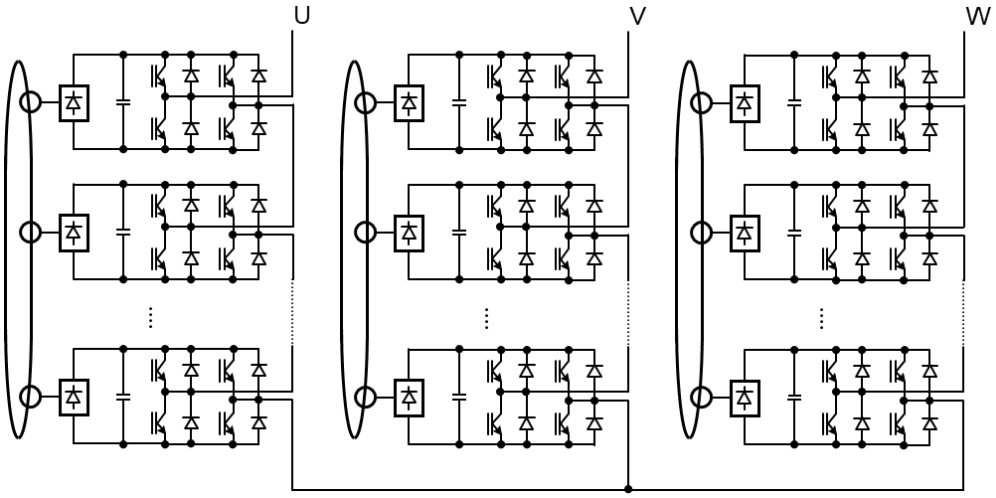

The rotor is bandaged with carbon fiber tape, reducing effective cooling. The rotor cooling mainly relies on airgap ventilation, severely limiting the dissipation of losses. In contrast to the asynchronous motor, the rotor of the PMSM does not require external excitation, which reduces the stator current on the one hand and renders the rotor of the PMSM largely free of current on the other. This reduces the motor and especially the rotor losses significantly. Considering an application of sinusoidal stator voltages the remaining losses in the rotor are caused by harmonics due to a non-sinusoidal flux distribution and saturation effects of the rotor construction holding the permanent magnets. However, harmonics generated by the inverter significantly amplify the rotor losses. The THD of the current needs to be below 2%. As the inverter needs to generate up to 333.4Hz frequency, the inverter needs to either be a multilevel inverter with sufficient switching frequency or some kind of output filter needs to be used [1, 2].

The here presented cascaded H-bridge inverter (CHB) is capable to generate nearly sinusoidal output voltages with an efficiency comparable to 3-level medium voltage inverters, for example. Each H-bridge comprises two phases, commonly designed in 2-level technology (see figure 2). The H-bridges are fed via a transformer secondary winding with a 6-pulse rectifier. Due to the series connection of many H-bridges, the feeding transformer is equipped with many secondary winding systems and thus becomes quite complex. Further, the transformer needs to be mounted close to the H-bridges to avoid huge cable efforts. These are the main disadvantages of this topology. On the other hand, there are many advantages like

- low harmonics on the grid side,
- low harmonics on the motor side,
- simple implementation of an H-bridge redundancy.

With N H-bridges the phase-to-phase voltage on the motor side and the rectifier pulses reach the following values

$$N_{motor} = 4\,N - 1 \quad (1)$$

$$f_{swph} = 2\,(N-1)\,f_{sw} \quad (2)$$

$$N_{grid} = 6\,N \quad (3)$$

where

N	Number of H-bridges in one phase;
N_{pp}	Number of voltage levels of phase-to-phase motor voltage;
f_{sw}	Switching frequency of device (IGBT)
f_{sw_pp}	Switching frequency phase to phase
N_{grid}	Number of pulses of rectifier on the grid side.

The high number of pulses of the rectifier at the grid side are reached by the phase displacement of the transformer secondary windings. If the switching frequency f_{sw} is selected to be 1kHz, the resulting switching frequency for the output voltage with N=9 is 32kHz. This is more than enough to generate the desired low harmonic output voltage. However, if each H-bridge is operated with a switching frequency of only 500Hz, only a few switching events per fundamental of the output voltage take place, which can lead to aliasing effects. To exclude negative effects, the prototype tests have been done with 1kHz switching frequency. Further investigations show that lower switching frequencies are also possible if the aliasing effects are managed.

The CHB inverter used for feeding the PMSM motor has N=9 H-bridges for 10kV output voltage and a power of 6MW (table 2). Tests have shown that the inverter prototype (figure 3) has significant margin as the power part could also run with 9MW. Thus, the future inverters for this power range will be significantly smaller.

Fig. 3 Cascaded H-bridge inverter (N=9), 10kV, 6MW

Rated apparent power	6.9	MW
Rated power	6.3	MW
Rated stator voltage	10	kV
Rated stator current	400	A
Maximum output frequency	600	Hz
Switching frequency of devices	0.5 to 1	kHz
Number of power cells per phase	9	
Water cooling temperature	5…40	°C
Overload (60sec)	120	%

Table 2 CHB inverter datasheet

Figure 4 gives an impression of the typical internal design of the inverter with the transformer on the left, the control in the middle and the H-bridges on the right. It can be seen that this inverter is equipped with 8 H-bridges per phase and it is completely air cooled.

Fig. 4 Cascaded H-bridge inverter

III. PMSM MOTOR CHARACTERISTICS AND CONTROL

The implemented high-speed control follows the standard structure of a flux-oriented control [3], which is not the primary focus of this paper. Consequently, only select aspects of the control are briefly outlined.

For the control of the motor, it is important to know how the stator inductances are depending on the stator currents as this influences the flux and voltage equations and consequently the control. With the assumption that the derivative of the synchronous inductances can be neglected the differential equation of the current is

$$u_d = R_s\, i_d + L_d \dot{i}_d \; - \; \omega_{rs}\, L_q\, i_q \tag{4}$$

$$u_q = R_s\, i_q + L_q \dot{i}_q + \omega_{rs}\, L_d\, i_d + \omega_{rs}\, \psi_m \tag{5}$$

where

u_d, u_q	stator voltage (d- and q-axis)
i_d, i_q	stator current (d- and q-axis)
L_d, L_q	stator inductance (d- and q-axis)
ω_{rs}	angular velocity of rotor to stator
ψ_m	permanent magnet rotor flux linkage

With a finite element modeling in 2D the following results have been calculated (Figure 5). It shows that the saturation effects are not very strong. This means that this dependency is of less importance for the dynamic control behavior but has an impact on the operation point optimization. Further, for these types of motors the saturation effects are not sufficient to use typical rotor identification methods for starting the motor without encoder. As the target application of this drive are high speed compressors or fans, the motor startup is typically not facing a high load torque. This allows to startup the motor with a simple injection of current to a low speed at which point the speed observer smoothly takes over.

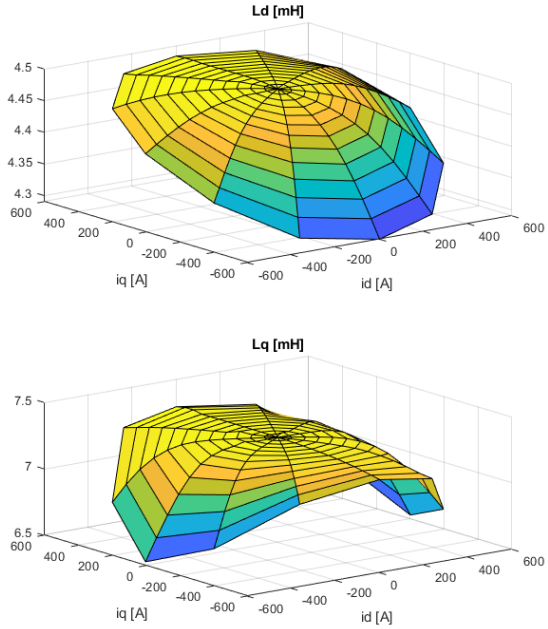

Fig. 5 Stator inductances in dependency of the current in synchronous coordinates (d,q)

As the output frequency of the inverter needs to be quite high and the harmonic requirements are very restrictive, the pulse pattern modulation is a critical aspect of the control. Each sampling instant, the control generates a reference modulation vector which is used to generate the pulse patterns for all the H-bridges for the following sampling interval. Thus, the voltage reference is a step function, which is visible in the harmonic spectrum of the output voltage. The control runs with a sampling frequency of 8kHz. This is high enough to reduce the resulting current harmonics to a low value. It further allows for a good compensation of dead time effects of the inverter.

IV. TEST RESULTS

For testing the drive system two PMSM motors were built, one with sleeve bearings and one with active magnetic bearings. One PMSM was fed by the inverter and the other one was loaded with a load bank (see fig. 6). No filter on the motor side is needed as the output voltage of the inverter is almost sinusoidal. Due to constraints of the test facility the load was limited to a power of 3MW.

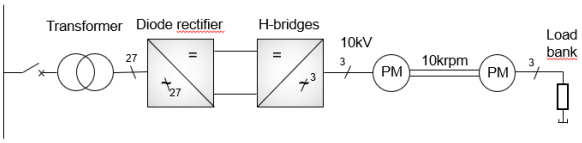

Fig. 6 Test setup

Figure 7 shows the two PMSM motors coupled for the tests. Each of the motors was tested feeding it with the inverter and loading it with the load bank.

Fig. 7 Coupled PMSM motors for test (active magnetic bearing control and motor on the left, sleeve bearing motor on the right)

The motors were fully tested in the whole speed range of up to 10000rpm and with a load of up to 3MW. During these tests the vibrations of the bearings of both motors were monitored in horizontal, vertical, and axial direction. For no load, the vibrations of the motors are below 0.55 and fulfill the SNAS and CMA standards. Figure 8 shows the velocities measured with the active magnetic bearings at 3MW load and 10000rpm.

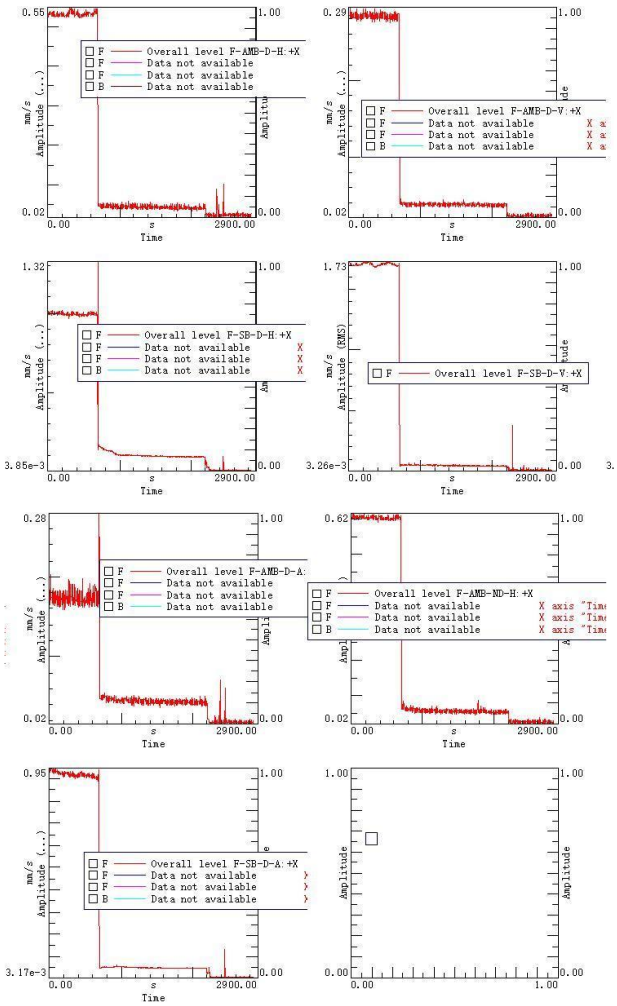

Fig. 8 Vibration measurements of the AMB in horizontal, vertical and axial direction at 3MW, 10000rpm

The measurement results of the load tests are summarized in table 3 showing that the vibrations stay below 2.8mm/s as a typical limit, even at this high speed of 10000rpm. These results confirm that the motors can easily meet the vibration requirements of high-speed applications.

Velocities (rms) [mm/s]	AMB PMSM	Sleeve baring PMSM
Horizontal	0.55	1.32
Vertical	0.29	1.73
Axial	0.29	0.95

Table 3 Measured maximum vibrations of the axes of the active magnetic bearing PMSM and sleeve baring PMSM over the whole speed range with up to 3MW load @ 10000rpm (values are velocities in [mm/s])

Figure 9 shows the stator voltage and phase currents of the motor at steady state with nominal speed and 3MW load. The output voltage is almost sinusoidal but shows the small steps caused by the sampling time of the control. As the resulting harmonics in the motor current are very small and don't dominate the overall THD, a further improvement is not a priority (Figure 10). The lower order harmonics like the 5th and 7th are more dominant and are mainly caused by the blanking times of the inverter, even though a blanking time compensation is already implemented on the central control level. As shown in the harmonic spectrum, the current THD is only 1% of the nominal current and with this fully sufficient for the PMSM motor.

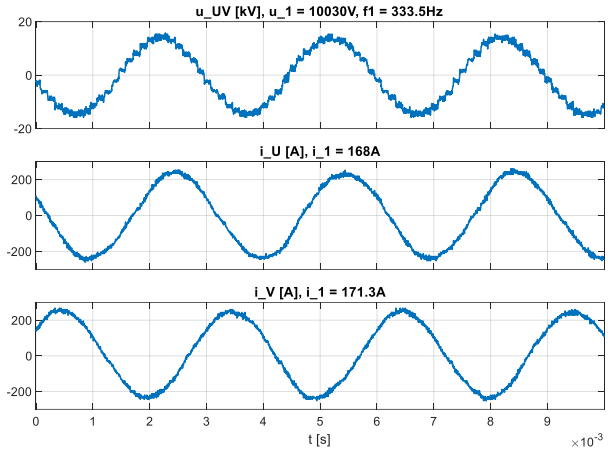

Fig. 9 Measured stator phase to phase voltage and currents of PMSM motor at 333.4Hz and 3MW load

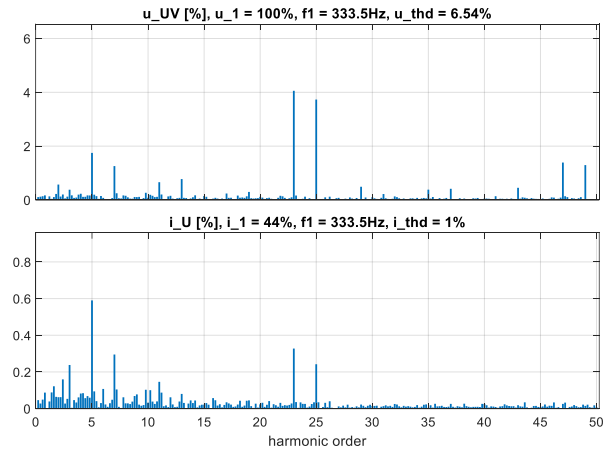

Fig. 10 Harmonic spectrum of measured stator voltage and current of PMSM motor at 333.4Hz and 3MW load

All the analysis of the drive system would not have been possible without a detailed simulation of the power electronics and the motor. With N=9 H-bridges, the power part has 108 IGBTs and diodes, 162 rectifier diodes, 27 dc links and a complex transformer. Only a detailed simulation considering all components, semiconductor blanking times and other effects allowed to commission the prototype with minimal tuning on site. The figures 11 and 12 show the simulation of the tested operating point with very good match of the measurements (figures 9 and 10).

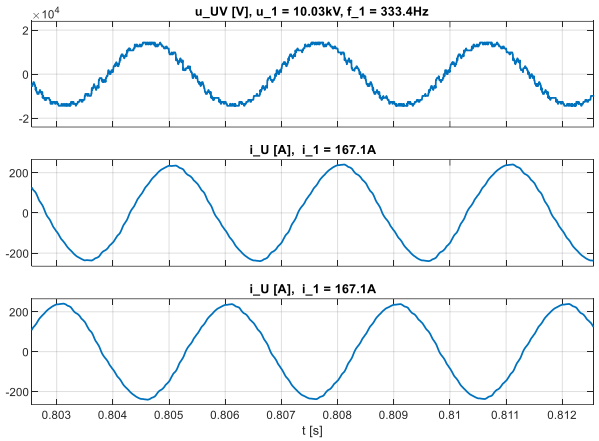

Fig. 11 Simulation of stator phase to phase voltage and currents of PMSM motor at 333.4Hz and 2800kW load

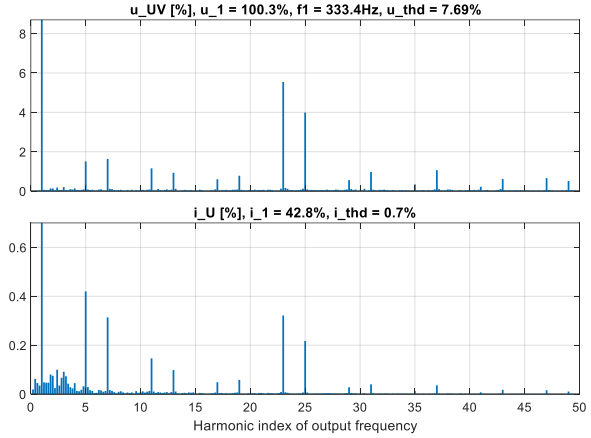

Fig. 12 Simulation of harmonic spectrum of voltage and current of PMSM motor at 333.4Hz and 2800kW load

The PMSM motor was simulated in detail with FEM tools to analyze the performance, losses, and cooling. Based on the geometric model a mesh model was generated and used for electromagnetic and thermal simulations (figure 13). All tested operating points up to 3 MW were compared with the simulation results (figure 14) and a good match between the measurement and simulation was achieved. After calibration of the model, temperature deviation of less than 5% have been reached. With this simulation model it was validated, that the nominal operation point of the PMSM fulfills the thermal design requirements.

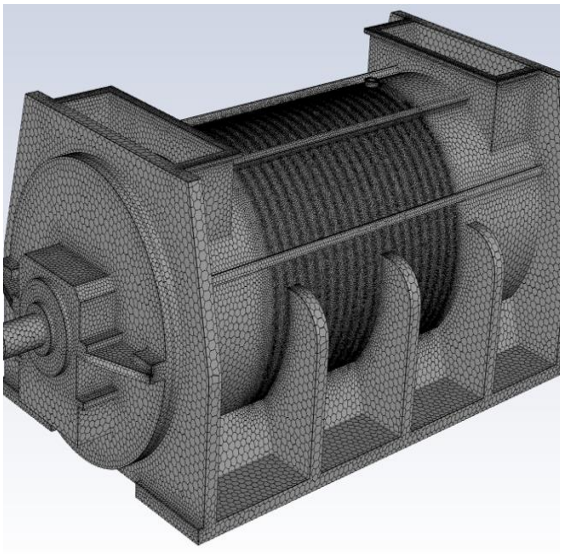

Fig. 13 Mesh model of the PMSM

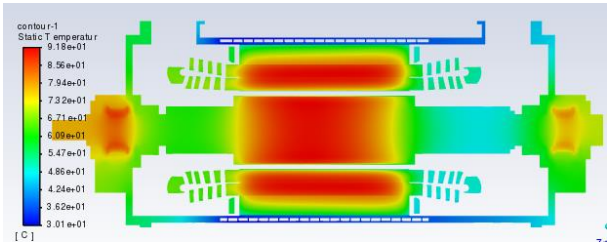

Fig. 14 Thermal simulation of the PMSM at 3MW (water inlet temperature 30°C, air inlet temperature 40°C)

The losses of the PMSM have been tested with the same method by comparing the measurements with the calibrated simulation. The PMSM reaches losses of below 2% at rated speed and load. This is at least 1% better than high speed induction motors which typically have an efficiency of about 97% [1]. Which technology is used, needs to be carefully analyzed for the individual application. Table 4 tries to give an indication of a loss comparison of the here presented PMSM drive system with a high-speed induction motor fed by an NPC inverter with a small output filter [2].

Efficiency	induction motor, NPC inverter, filter	PMSM motor, CHB inverter, no filter
Transformer	0.99	0.988
Power part	0.982	0.985
Filter	0.99	0.
Motor	0.97	0.982
Total	0.934	0.956
Total losses	427kW	279kW

Table 4 Efficiency comparison of PMSM and CHB inverter with conventional induction motor drives

The difference of 148kW in the losses shows the potential of the PMSM drive system in reducing CO2 emissions. It also reduces the OPEX per anno by about 190k€ if 0.16€ are assumed as energy cost.

V. RELIABILITY

As the cascaded H-bridge inverter is built of many series connected H-bridges, one could assume that the reliability of the inverter is lower than an inverter with large devices like a 3-Level inverter. The reliability of the CHB inverter is strongly dependent on the reliability of the applied H-bridge. In critical applications such as gas compressors, achieving a level of reliability beyond standard requirements is in any case mandatory, which can usually only be reached with redundancy. With the CHB inverter topology redundancy of the power part is quite simple to be achieved by bypassing a failed H-bridge with a bypass switch (Fig. 15). Each H-bridge is monitored by the control. If an anomaly occurs, the warning or error message is sent to the central control. In case of a serious fault, the inverter may shortly interrupt the operation to check the status of the drive. The faulty H-bridge is bypassed with the switch and the operation is continued. The drive control doesn't request an interruption of the operation.

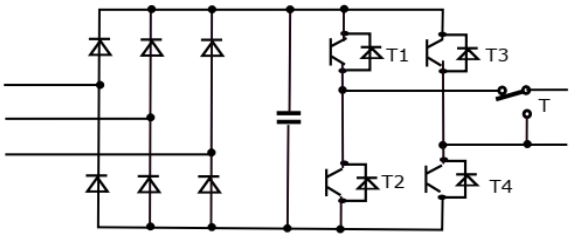

Fig. 15 H-bridge with bypass switch for redundancy

The reliability of the system with active redundancy can be evaluated by applying the probability function of the Binomial distribution. It describes the probability of getting exactly k successes in n independent Bernoulli trials with the probability p [4]:

$$f(k,n,p) = \binom{n}{k} p^k \, (1-p)^{n-k} \tag{6}$$

where

k	number of the successes (failures);
n	number of modules per phase;
p	probability of H-bridge failure.

For calculating the reliability of the inverter power part, one phase of the inverter is running without fault if at least M of N cells are operating correctly. This means the reliabilities for each case of k = M to k=N needs to be added. After this the resulting reliability is taken by the power of three for the three phases:

$$R_{ppart}(t) = \left(\sum_{k=M}^{N} \binom{N}{k} R_{cell}(t)^k \left(1 - R_{cell}(t)\right)^{N-k} \right)^3 \tag{7}$$

where

R_{cell}	Reliability of H-bridge;
R_{ppart}	Reliability of complete power part.

In addition to the power part other parts of the inverter like the control, circuit breaker, cooling, transformer, and other auxiliaries need to be considered.

For the analysis of the reliability typical values of the FIT rates of the various components have been used [4]. The calculation shows that the redundancy of the H-bridges significantly increases the overall reliability to up to 11 years for the power part in case of two redundancies (figure 16).

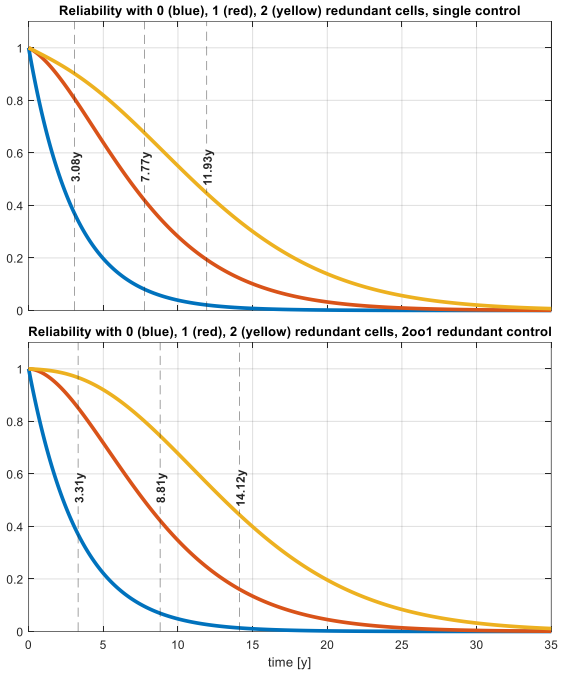

Fig. 16 Reliability of power part and complete inverter with 0, 1 and 2 redundant H-bridges

Even without installing redundant power cells the inverter can operate closely to 100% power if one power cell fails. This is achieved by displacing the common mode system of the output voltage modulation. Figure 17 shows the output voltage vectors of the inverter in the Clarke transform coordinates in case of failed H-bridges. Without failure the black hexagon is the available voltage area of the inverter. Due to the failed H-bridges the area is reduced to the blue hexagon. The red lines symbolize the maximum voltage vectors in each phase. The blue hexagon is becoming asymmetrical. If the output voltage shall still be sinusoidal, the modulation now needs to be within the green circle.

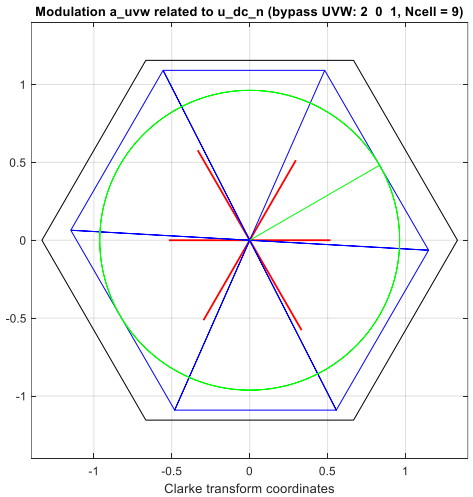

Fig. 17 Output voltage Clarke transform in case of 2 failing H-bridges in phase U and 1 failing in phase W

With this assumption the reduced output voltage can be calculated for different cases of failed H-bridges. Table 5 shows that the resulting voltage reduction is less than the reduction of the individual phase voltages. For example, if one H-bridge fails in phase W, the resulting reduction of the available voltage amplitude is only reduced by 5.6% while the phase W is reduced by 11%.

U	V	W	a_v_red	a_w_red	a_red
0	0	1	1.000	0.889	0.944
0	0	2	1.000	0.778	0.889
0	0	3	1.000	0.667	0.833
0	1	1	0.889	0.889	0.889
0	1	2	0.889	0.778	0.833
0	1	3	0.889	0.667	0.778

Table 5 Failed H-bridges in U,V,W and resulting reduction of modulation in V,W and the total available modulation a_red (N=9 without redundancy)

In case of no redundant H-bridges, the motor can still operate with 5.6% less voltage after one H-bridge has failed. In many applications this voltage reduction can be compensated by a slightly higher stator current for weakening the stator flux of the PMSM and keeping the nominal torque. With additional H-bridges as redundancy a fault of cause has no impact on the operation.

VI. GRID FAULT RIDE THROUGH

A critical aspect of non-interrupted drive train operation is the capability of riding through grid voltage dips. A grid fault ride through is always feasible if the drive train has sufficient inertia, so that the operation speed is not dropping critically while the voltage is dropping below 80% of the nominal voltage. Most of the grid codes specify a recovery of the voltage within 1.5 seconds, some recover only after 3 seconds.

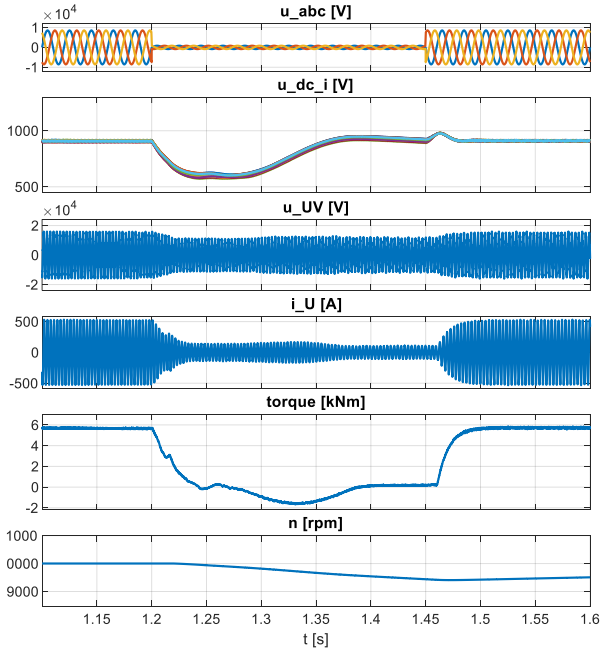

Fig. 18 Grid fault ride through of a voltage dip down to 15%, 250ms, inertia assumed

As the here presented drive has rectifier bridges and no active front end on the input, it can only ride through a grid fault by directly reducing the delivered torque to stabilize the dc link voltage. In case of a sudden drop to below 20% the torque drops to zero and the kinetic energy of the drive train needs to support the dc link during the voltage dip.

Figure 18 illustrates the behavior of the drive during voltage dips. When the three-phase grid voltage u_abc dips to below 20%, the individual dc link voltages u_dc_i quickly drop. In case of the N=9 CHB inverter 27 dc link voltages are existing. The motor torque must be quickly reduced, transitioning into a generative mode for a short duration to recover the dc links. After this the torque is maintained close to zero until the grid voltage recovers. Once the grid voltage recovers, the control returns to the original operation point and accelerates the motor back to the original operation point. The acceleration is not depicted anymore, as this spans significantly longer than the dip.

VII. PREDICTIVE MAINTENANCE

The monitoring and predictive maintenance of drive trains is of increasing relevance for highly reliable applications. Often, cost constraints are limiting the amount of applied sensors. As a standard, the digital drive system already measures many physical values like the motor voltages and currents, all dc link voltages, power cell temperatures and the line voltages and currents. This data can be used for the analysis of the power electronics of the inverter and identification of weaknesses to initiate predictive maintenance. Examples for power electronics fatigues are the dc link capacitor aging or semiconductor weaknesses which might show an increase in the collector-emitter cut-off currents in the power cells.

As an additional feature, the drive control can also be equipped with an interface to directly connect vibration sensors mounted on the drive train. The vibration sensors are connected via the IEPE interface and can be acquired synchronously with the other measurement data of the inverter and with 10kHz bandwidth. As an option, vibrations sensors also have an integrated temperature measurement. This saves wiring and the temperature measurement can be additionally used to compensate temperature effects in the sensor (Figure 19).

Fig. 19 Wired IEPE vibration sensor with integrated temperature sensor for screwed mounting

With this, the drive including the load can be analyzed in combination with all the other measurement data of the inverter. This builds the future for the analysis of the system status with the inverter control or in the cloud once the data is uploaded. A cloud-based system can be utilized for the analysis of the health status of the system and predictive maintenance. Here are some examples of failure modes of the PMSM drive train which can be monitored based on the measurements:

- asymmetrical demagnetization of the rotor,
- displacement of the air gap,
- partial short circuit of a stator winding,
- bearing damages
  (defective balls, outer race, inner race, cage)
- load side eccentricities.

New drive installations more and more foresee a connection of the drive to a local server or cloud system with cyber security protection. With the acquisition of the vibration sensors via the drive control additional efforts for wiring and installation of specific data devices can be saved.

VIII. CONCLUSIONS

A new medium voltage high speed drive train with a 6MW PMSM motor has been presented. The test results have successfully validated the design and the drive train is capable to deliver the nominal power at 10000rpm. The motor can be built with sleeve bearings or with active magnetic bearings with very good vibration results. The drive train including the grid transformer reaches an overall efficiency of 95.6% due to the highly efficient permanent magnet technology and the low current THDi of less than 2% without any filter. With this, the drive train is clearly leading in technology and a new benchmark in efficiency.

The drive can be optionally built with redundant power cells (H-bridges) which are bypassed in case of failure. This strongly increases the reliability of the drive system. However, is has been shown that even without additional power cells the bypass function is very beneficial as it allows to continue operation with slightly reduced output voltage if one power cell fails.

For the analysis of the drive train a very detailed simulation model has been built. Off-line simulations match measurements with good accuracy and make an off-line tuning of the drive possible. This model can also be used to build a digital twin for monitoring and predictive maintenance. A simplified simulation is already implemented on the control hardware and allows the user to operate the inverter without power for pre-commissioning. Furthermore, additional vibration and temperature sensors can be seamlessly integrated into the drive control and all measured data is synchronously acquired and stored into datasets to be uploaded on servers or the cloud. With this the drive system is prepared to become fully digital.

IX. ACKNOWLEDGEMENTS

We acknowledge and thank Prof. Dr. Salama for his strong support in the modelling of the inverter topology considering all details of the power electronic devices while keeping a fast execution time of the simulations [5]. He also supported the project with his vast experience in power electronics.

X. REFERENCES

[1] Manfred Nahrstaedt, Ulrich Putz, Detlef Wendt, “High Speed, high Power Compressor Drives with Medium Voltage Induction Motors”, EPE, 2001

[2] Jörg Janning, Jean-Charles Mercier, “Medium Voltage Three-Level Inverter for High Speed Applications”, EPE, 2007

[3] Klaus Peter, Fabian Mink, Joachim Böcker, “Model-Based Control Structure for High-Speed Permanent Magnet Synchronous Drives”, IEEE (IEMDC), 2017

[4] Saleh Farzamkia, Hossein Iman-Eini, Arash Khoshkbar-Sadigh, Mehdi Khaleghi and Masoud Noushak, “Comparative and Quantitative analyze on Reliability of MMC-Based and CHB-Based Drive Systems Considering Various Redundancy Strategies” in IEEE, 2020.

[5] Samir Salama, “Fixed Admittance Matrix Technique for Real Time Power Electronics Simulation on Matlab/Simulink”, PCIM Europe, 2021

XI. VITA

Dr. Jörg Janning graduated from the University of Dortmund 1989 with diploma in electrical engineering. He was working as researcher in the Daimler-Chrysler institute until 1998 focussing on control of power electronics for the industry and railway. In 1997 he received his doctorate in electrical engineering at the TU Clausthal. He joined ALSTOM managing drive control systems, then got promoted as R&D leader of Converteam in 2004. At GE Power Conversion he got awarded 2012 to the Chief consulting engineer of Power Conversion, led the engineering departments of power electronics and industry systems. 2018 he became the CTO of GE Power Conversion for the CEER region. End of 2019, he joined Wolong Global Research as CTO for power electronics. Jörg has published more than 30 papers and holds more than 30 international patents in the areas of drives, power electronic applications and control in many fields of the industry, renewables energy, storage systems and power conversion. Jörg is IEEE member.
Joerg.janning@wolong.com

Dr. Zhu Peng Cheng received the M.A.Sc. and Ph.D. degrees in power electronics and electric drive from the Huazhong University of Science and technology, Wuhan, Hubei, China, in 2002 and 2006, respectively. He joined GE Global Research Center, Shanghai, in 2006, where he took positions as senior enginer, manager of power conversion circuits lab and program manager of SiC. He joined SEMIKRON Electronics, Zhuhai, in 2017, where he took position as director of automotive. Since 2020, he joined Wolong Electric, where he is currently Chief Engineer of Wolong Drive Division. He has published more than 20 technical articles, and holds more than 10 granted/pending U.S./European patents in the areas of power conversion, medium-voltage drives, and renewable

energy systems. Pengcheng Zhu is also a member of China Power Supply Society (CPSS) and IEEE.
zhupengcheng@wolong.com

Dr. Chunzhi Deng received the M.A.Sc. degrees in Mechanical Engigeering from the LanZhou University of Science and technology, LanZhou, GanSu, China, in 2009. He joined Dun'An electric company, Xi'An, China in 2009, where he took positions as senior enginer mainly focus on the Double Fed Generetor design. He joined Siemens Global Research Center, Xi'An, in 2013, where he took positions as team leader mainly focus on high voltage motor deisign. Since 2019, he joined Wolong Electric, where he is currently Chief Engineer of Wolong Global Research Center. He has published more than 8 technical articles, and holds more than 40 granted/pending China/U.S./European patents in the areas of motor related topics. Chunzhi Deng is also a member of Chinese Society for Vibration Engineering(CSVE) and IEEE.
dengchunzhi@wolong.com